Research Square

Preprints are preliminary reports that have not undergone peer review.
They should not be considered conclusive, used to inform clinical practice,
or referenced by the media as validated information.

A humidity-buffering and visually indicative wood substrate for passive microclimate control in museum display cases

Lin Shi
Central South University of Forestry and Technology
Ting He
Central South University of Forestry and Technology
Guangyao Cui
The Palace Museum
Li Zeng
t19911929@csuft.edu.cn

Central South University of Forestry and Technology

Article

Keywords:

Posted Date: August 24th, 2026

DOI: https://doi.org/10.21203/rs.3.rs-10672427/v1

License: This work is licensed under a Creative Commons Attribution 4.0 International License.
Read Full License

Additional Declarations: No competing interests reported.

Version of Record: A version of this preprint was published at npj Heritage Science on November 14th, 2026. See the published version at https://doi.org/10.1038/s40494-026-03116-z.

A humidity-buffering and visually indicative wood substrate for passive microclimate control in museum display cases

Lin Shi[1], Ting He[1], Guangyao Cui[2], Li Zeng[1*]

[1]Central South University of Forestry and Technology, Changsha, 410004, China

[2]The Palace Museum, Beijing 100009, China

[*]Corresponding author, E-mail: t19911929@csuft.edu.cn

Abstract: Eco-friendly substrates combining passive humidity regulation with visual indication remain limited for enclosed museum display cases. Poplar wood was modified by low-temperature ultrasonic co-impregnation with glycerol and anthocyanin. Substrate screening, single-factor tests, and orthogonal experiments quantified the effects of additive dosage and impregnation time on weight percent gain, dimensional stability, and humidity-responsive color change. SEM and FTIR indicated that modification was governed mainly by pore filling and intermolecular hydrogen bonding. The optimal process was 22 wt% glycerol, 0.6 wt% anthocyanin, and 9 h impregnation, yielding a 51% higher 24 h moisture uptake than untreated poplar, with effective pore filling and uniform pigment dispersion. The color response remained detectable after 30 wet-dry cycles. This work provides an environmentally compatible dual-functional wood substrate and a technical reference for passive humidity-buffering and visual monitoring in enclosed exhibition spaces, providing an effective tool for the preventive conservation of wooden heritage artifacts.

Introduction

Coastal and southern China are often exposed to sustained and sharply fluctuating humidity, which commonly causes damp interior walls, mildew growth, and moisture-related problems in wooden floors. Such conditions also create substantial risks for wooden cultural relics stored in sealed museum repositories and display cabinets [1]. Because wooden relics are porous and highly hydrophilic, unstable high-humidity microenvironments can accelerate irreversible deterioration. At present, humidity-buffering in museum storage spaces still relies mainly on electromechanical devices [2,3]. These systems require high energy input, may respond slowly, and can generate uneven humidity fields. Airflow from such equipment may also disturb fragile relics, whereas repeated cabinet opening for humidity monitoring disrupts the stable internal microclimate. Single-function humidity-buffering materials or chemical humidity indicators cannot simultaneously provide passive buffering and safe visual monitoring in closed exhibition environments. Accordingly, passive wood-based materials that combine humidity buffering with visual humidity indication are valuable for developing functional interior components for display cabinets. In this context, modified wood prepared through mild and environmentally compatible processes with excellent high-humidity moisture absorption performance has practical and engineering significance for indoor damp-proofing and as a passive microclimate management substrate for museum enclosures in humid regions [4-6].

Previous studies have investigated moisture-proof materials for high-humidity environments [7-9]. The main strategies include high-temperature modification, chemical impregnation, and surface coating [10]. However, high-temperature treatment may damage the fibrous structure and

natural morphology of wood and alter its physicochemical properties [11]. This is difficult to reconcile with the authenticity principle of heritage conservation and is therefore unsuitable for use in conservation-grade materials for heritage display environments. Conventional chemical modification commonly depends on reagents that leave substantial residues and show limited environmental compatibility, restricting their use in enclosed storage environments and indoor spaces. Traditional soaking under ambient or low-temperature conditions causes relatively limited damage and has been widely used in relic conservation, but it remains constrained by slow penetration, uneven impregnation, and surface-localized loading of functional components. These limitations often result in weak humidity-regulation capacity and poor durability, especially under sharp humidity fluctuations [12-15]. In addition, the theoretical basis of humidity-buffering in wood remains incomplete. Existing studies usually examine glycerol-based humidity-buffering wood and anthocyanin color-changing substrates separately; green low-temperature composite systems that integrate passive humidity buffering with minimally invasive visual monitoring remain scarce. The lack of matched solvent-optimization strategies to suppress pigment oxidation and uneven color dispersion further restricts the design of high-performance humidity-control protective materials [16-17].

To address these constraints, this study selected three commercial wood species, *Cunninghamia lanceolata* (Chinese fir), *Paulownia* spp. (paulownia), and *Populus* spp. (poplar), as substrates. Multifunctional modified wood was prepared by low-temperature ultrasonic-assisted impregnation in a green mixed solvent composed of anhydrous ethanol and deionized water. Citric acid was used to adjust the pH of the mixed impregnation solvent during specimen preparation. Glycerol was introduced to enhance humidity responsiveness and dimensional stability, whereas purple sweet potato anthocyanin was incorporated as a visual color indicator. Preliminary experiments evaluated the initial physical properties and microscopic pore characteristics of the candidate substrates. Single-factor experiments were then conducted using impregnation rate, weight percent gain (WPG), equilibrium moisture content (EMC), dimensional change rate, and surface color difference as evaluation indices to determine reasonable dosage ranges for the two additives. Orthogonal experiments were further designed with glycerol content, anthocyanin content, and impregnation duration as variables for combined process optimization. Dynamic moisture-absorption and cyclic humidity-aging tests were performed on the optimally modified specimens to clarify their high-humidity moisture absorption performance and long-term color reversibility under simulated museum storage conditions. Scanning electron microscopy (SEM) and Fourier transform infrared spectroscopy (FTIR) were used to examine the loading state of functional components and the modification mechanism through analyses of microscopic morphology and chemical functional groups. The proposed system is designed to impart multiple functions to wood. Purple sweet potato anthocyanin has antibacterial activity and a reversible humidity-responsive color change, enabling non-contact visual humidity monitoring in sealed cabinets. As a pH-sensitive natural pigment, anthocyanin can undergo reversible color changes in

response to moisture-content and surface-pH shifts driven by ambient humidity. Glycerol, owing to its strong hygroscopicity, further enhances the humidity response and helps stabilize the visual humidity indication of the modified wood [18-23].

This study systematically clarifies the relationships among impregnation parameters, functional additives, and the humidity-buffering and color-responsive performance of modified wood. The mild low-temperature ultrasonic co-impregnation strategy endows wood substrates with outstanding high-humidity moisture-uptake performance and visual humidity-sensing capabilities without damaging their inherent fibrous structure. The resulting modified wood can serve as a passive humidity-control substrate for museum display cabinets and as an indoor moisture-protection material for residential buildings and ancient architecture. This work provides a technical reference for developing eco-friendly functional wood materials aimed at passive microclimate regulation in heritage display environments [24,25].

Methods

Three commercial wood species, *Cunninghamia lanceolata* (Chinese fir), *Paulownia* spp. (paulownia) and *Populus* spp. (poplar), were selected for this study. For each species, logs were harvested from trees of similar age and trunk position within the same stand to minimize intraspecific variability. Raw materials were purchased from qualified suppliers, and wood species identification was verified by the Wood Anatomy Laboratory of Beijing Forestry University. The logs were sawn into lumber and air-dried at 20–28 °C and 50–70% RH until the moisture content stabilized at 8–10%, corresponding to the equilibrium moisture content (EMC) of indoor wood in southern China. The lumber was then conditioned at 25 ± 2 °C and 65 ± 5% RH for four weeks, after which defect-free, straight-grained specimens measuring 50 mm (radial) × 50 mm (tangential) × 10 mm (longitudinal) were prepared. Each test was performed in triplicate (n = 3). All data are reported as the mean ± standard deviation, and one-way analysis of variance (ANOVA) was used for comparisons among groups.

Specimens were polished successively along the grain using 120-, 240-, and 400-grit waterproof sandpaper to remove surface burrs, sawdust, and surface extractives and were then cleaned with anhydrous ethanol. The polished specimens were oven-dried at 103 ± 2 °C to constant mass (mass change < 0.2% over 24 h). The oven-dried specimens were cooled immediately to room temperature in a desiccator. Afterward, all specimens were conditioned at 25 ± 2 °C and 65 ± 5% RH for 48 h to stabilize their moisture content. Fixed positions were then marked on each specimen for dimensional measurements. The specimens were sealed and stored in the dark until impregnation.

Analytical-grade reagents were used throughout the experiment, including anhydrous ethanol, deionized water, glycerol, and purple sweet potato anthocyanin. Auxiliary supplies, including waterproof sandpaper, qualitative filter paper, conductive adhesive, and sealed sample bags, were also prepared and used. All instruments were calibrated before use. Detailed information on the

115 main equipment is listed in Table 1.

116 Table 1 Main instruments used in this study

Instrument	Model	Manufacturer
Electric oven	DH303	Hengda Instrument
Low-temperature ultrasonic cleaner	ZN-P	Hengda Instrument
FTIR spectrometer	Nicolet 6700	USA
Scanning electron microscope	ZEISS Sigma 500	Germany
Colorimeter	CR-400	Japan

117 All experimental procedures were conducted in accordance with the standards GB/T 1927.4–
118 2021 and EN 14734:2022 [26,27]. The base solvent was prepared by mixing anhydrous ethanol and
119 deionized water in a mass ratio of 55:10. Analytical-grade citric acid powder was added and fully
120 stirred to adjust the pH of the mixed solution to 4.5–5.5 [28,29]. Subsequently, glycerol and purple
121 sweet potato anthocyanins were added to the mixed solvent according to the experimental design
122 to form the impregnation solution. The entire impregnation process was maintained below 35 °C
123 to prevent reagent degradation and damage to wood fibers. An ultrasonic cleaner operating at a
124 fixed frequency of 80 kHz and constant output power was used. The treatment followed a cyclic
125 mode: 15 min of ultrasonic vibration, followed by 5 min of static immersion, with the cycle
126 repeated for a total processing time of 6 h. During treatment, all specimens were fully submerged
127 in the solution. After impregnation, residual liquid on the specimen surfaces was gently removed
128 using qualitative filter paper. The specimens were then left to stand at 25 ± 2 °C for 24 h until the
129 solvent had completely evaporated, after which all performance tests were conducted [30,31]. The
130 entire fabrication process is schematically shown in Fig. 1.

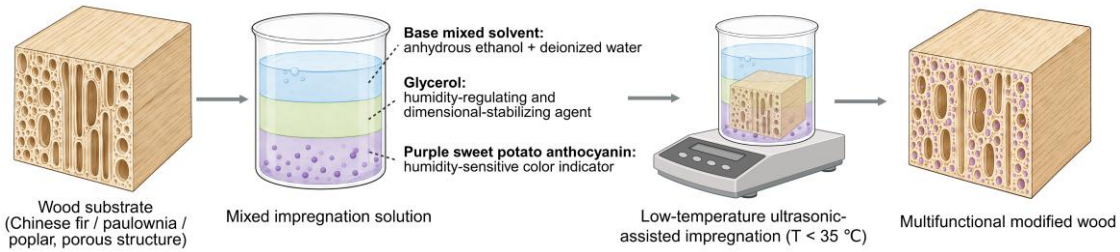


Fig. 1. Flowchart illustrating the fabrication procedure of multifunctional modified wood.

131 Preliminary Experiment

132 Preliminary experiments were conducted on Chinese fir, paulownia, and poplar to identify
133 the optimal wood substrate, in Fig. 2. A blank group and a pure-solvent group (impregnated solely
134 with the aforementioned base solution, free of glycerol and anthocyanins) were established for
135 each wood species, and three replicate specimens were cut from the same batch of defect-free
136 wood for each group. Specimens in the blank group received only pretreatment without
137 impregnation. The pure-solvent group was treated with the base solution without functional
138 additives under the standard impregnation parameters and operating procedures. All tests were
139 performed at 25 ± 2 °C and 65 ± 5% RH. For each impregnation duration (0.5, 1, 2, 4, and 6 h), a
140 separate group of three replicate specimens was prepared for each species. After the designated

time, residual liquid on the surface was rapidly wiped off, and the specimens were weighed immediately to calculate the impregnation rate. After standing for 24 h to allow complete solvent volatilization, the EMC and geometric dimensions of the specimens were measured. Unified criteria were applied for substrate screening. The wood species with a moderate pore structure, uniform impregnation behavior, minor dimensional variation, and stable surface color was selected as the substrate for subsequent formal experiments.

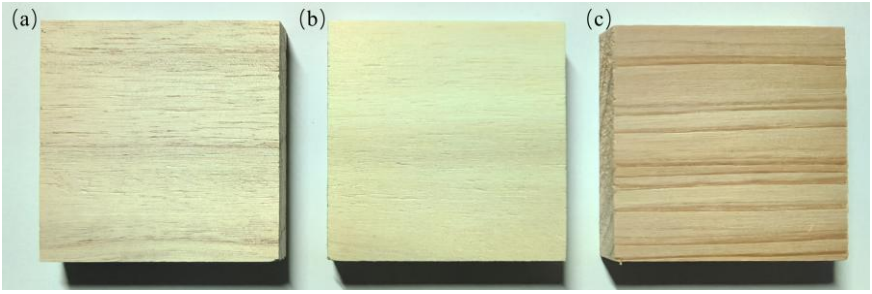


Fig. 2. Macro surface morphology of three wood substrates. (a) *Paulownia* spp.; (b) *Populus* spp.; (c) *Cunninghamia lanceolata* (Chinese fir).

Single-factor Experiment

Single-factor experiments were carried out for glycerol and purple sweet potato anthocyanin to determine the optimal dosage ranges of the functional additives in the impregnation system. The optimal wood substrate screened from the preliminary experiments was used, and the aforementioned base impregnation solution was adopted. Using weight percent gain (WPG), EMC, dimensional stability, and surface color difference as evaluation indices, the effects of additive dosage on the comprehensive properties of the modified wood were investigated. Appropriate dosage ranges were then determined to optimize the formulation of the impregnation solution.

All experimental gradients were determined from repeated preliminary impregnation trials. Glycerol at a dosage below 20 wt% produced a weak modification effect. When the glycerol content exceeded 28 wt%, the viscosity of the impregnation solution increased, which hindered the penetration of functional components. Accordingly, the glycerol gradient was set from 20 wt% to 28 wt%. For purple sweet potato anthocyanin, the color-indication performance was limited at dosages below 0.2 wt%, whereas precipitation tended to occur when the dosage exceeded 1.0 wt%. Therefore, the anthocyanin dosage was set within the range of 0.2–1.0 wt%. During the single-factor test of glycerol, the purple sweet potato anthocyanin content was fixed at 0.5 wt%. The detailed experimental schemes are presented in Tables 2–4, where x and y denote the optimal mass fractions of glycerol and anthocyanin, respectively, as determined sequentially from the single-factor tests.

Table 2 Experimental design for glycerol mass fraction

Test Samples	Formulation (glycerol mass fraction)
1	Base solution (55 wt% anhydrous ethanol + 10 wt% deionized water)
2	Base solution + 0.5 wt% purple sweet potato anthocyanin
3	Base solution + 0.5 wt% purple sweet potato anthocyanin + 20 wt% glycerol

4	Base solution + 0.5 wt% purple sweet potato anthocyanin + 22 wt% glycerol
5	Base solution + 0.5 wt% purple sweet potato anthocyanin + 24 wt% glycerol
6	Base solution + 0.5 wt% purple sweet potato anthocyanin + 26 wt% glycerol
7	Base solution + 0.5 wt% purple sweet potato anthocyanin + 28 wt% glycerol

Note: Sample 1 served as the blank control group, and Sample 2 served as the reference control group. Samples 3–7 corresponded to groups with different glycerol dosages. Three replicate specimens were prepared for each group. The optimal glycerol mass fraction determined from this experiment is denoted as x in subsequent tables. Objective: to determine the optimal glycerol mass fraction x.

Table 3 Experimental design for purple sweet potato anthocyanin mass fraction

Test Samples	Formulation (purple sweet potato anthocyanin mass fraction)
1	Base solution (55 wt% anhydrous ethanol + 10 wt% deionized water)
2	Base solution + x glycerol
3	Base solution + x glycerol + 0.2 wt% purple sweet potato anthocyanin
4	Base solution + x glycerol + 0.4 wt% purple sweet potato anthocyanin
5	Base solution + x glycerol + 0.6 wt% purple sweet potato anthocyanin
6	Base solution + x glycerol + 0.8 wt% purple sweet potato anthocyanin
7	Base solution + x glycerol + 1.0 wt% purple sweet potato anthocyanin

Note: Sample 1 served as the blank control group, and Sample 2 served as the reference control group, where x is the optimal glycerol mass fraction determined from Table 2. Samples 3–7 corresponded to groups with different anthocyanin dosages. Three replicate specimens were prepared for each group. The optimal anthocyanin mass fraction determined from this experiment is denoted as y in the subsequent table. Objective: to determine the optimal anthocyanin mass fraction y.

Table 4 Compound formulation test design

Test Samples	Formulation
1	Base solution + x glycerol + y purple sweet potato anthocyanin

Note: x and y denote the optimal mass fractions of glycerol and anthocyanin determined from Tables 2 and 3, respectively. Objective: To verify the combined performance of the optimised formulation.

Orthogonal Experiment

Based on the single-factor experimental results, three factors, namely glycerol mass fraction, purple sweet potato anthocyanin mass fraction, and impregnation time, were selected, and three levels were set for each factor. The level values were determined from the single-factor and preliminary experimental results. An $L_9(3^3)$ orthogonal array was used for experimental design. All specimens were prepared with uniform dimensions of 50 mm × 50 mm × 10 mm, and three replicate specimens were used for each test group.

The pretreatment procedure was the same as that in the single-factor experiment. Samples

were conditioned at 25 ± 2 °C and 65 ± 5% RH for 48 h to achieve an EMC of 8%–10%, ensuring uniform moisture distribution and providing a stable initial state for color measurement. The initial color parameters of each specimen were recorded under these standard conditions as the baseline. All tests were conducted at a constant temperature of 25 °C and 80% RH to eliminate environmental interference. Specimens were placed in this high-humidity environment until their mass change within 24 h was less than 0.2% of the total specimen mass (i.e., reaching moisture equilibrium), after which surface color parameters were measured. The total color difference ΔE^*_{ab} was used as the primary evaluation index, with weight percent gain (WPG) and EMC serving as auxiliary indices. The influence of each factor was assessed using range analysis and one-way ANOVA to determine the optimal process parameters. Factor levels and the orthogonal experimental design are shown in Tables 5 and 6, respectively.

Table 5 Factors and levels of orthogonal experiment

Level	Factor A (Glycerol mass fraction)	Factor B (Purple sweet potato anthocyanin mass fraction)	Factor C (Impregnation time)
1	21 wt%	0.5 wt%	3 h
2	22 wt%	0.6 wt%	6 h
3	23 wt%	0.7 wt%	9 h

Table 6 Orthogonal experimental design

No.	Factor A	Factor B	Factor C
1	1	1	1
2	1	2	2
3	1	3	3
4	2	1	2
5	2	2	3
6	2	3	1
7	3	1	3
8	3	2	1
9	3	3	2

Experimental Methods

The impregnation rate and dry weight percent gain (WPG) of specimens were measured by weighing. Before testing, all pretreated specimens were conditioned at 25 ± 2 °C and 65 ± 5% RH until mass stabilization, and the initial reference mass (m0) of each specimen was recorded to a precision of 0.01 g. For unmodified and pure-solvent groups, m0 was defined as the oven-dry mass. For modified groups, because glycerol and anthocyanin are nonvolatile and heat-sensitive, m0 was defined as the mass after conditioning at 25 ± 2 °C and 65 ± 5% RH prior to impregnation. Specimens were fully immersed in the impregnation solution and treated under the established low-temperature ultrasonic procedure. They were withdrawn after 0.5, 1, 2, 4, and 6 h of

impregnation. After residual surface solution was quickly removed with qualitative filter paper, the specimens were weighed immediately to record the mass at each time point. Three replicate specimens were prepared for each group, and the results are reported as the arithmetic mean.

The impregnation rate, defined as the solution uptake per unit specimen surface area per unit time, was calculated using Equation (1). The final dry weight percent gain, which reflects the actual loading of functional components in the wood, was calculated using Equation (2):

$$v = \frac{m_t - m_0}{A \times t} \tag{1}$$

where v is the impregnation rate in g/ ($m^2 \cdot$ h); m_t is the specimen mass at time t in g; m_0 is the initial reference mass of the specimen in g; A is the total surface area of the specimen in m^2; t is the impregnation time in h.

$$W = \frac{m_6 - m_0}{m_0} \times 100\% \tag{2}$$

where W is the dry weight percent gain of the specimen in %; m_6 is the equilibrium mass of the specimen after 6 h impregnation and 24 h standing for complete solvent volatilization in g; m_0 is the initial reference mass of the specimen in g.

This test was designed to examine the equilibrium moisture-absorption behavior of modified wood and to evaluate the effect of additive content on humidity-regulation capacity. Because purple sweet potato anthocyanin is thermally unstable and glycerol is volatile, specimens from the blank and pure-solvent groups in the preliminary experiments were oven-dried at 103 ± 2 °C to constant mass. By contrast, specimens for the single-factor and orthogonal tests were conditioned at 25 ± 2 °C and 65 ± 5% RH. All weighing operations were performed to an accuracy of 0.01 g, and three replicate specimens were used for each group. Conditioning was considered complete when the mass change within 24 h was less than 0.2% of the total specimen mass. EMC was calculated using Equation (3):

$$EMC = \frac{m_e - k}{k} \times 100\% \tag{3}$$

where *EMC* is the static equilibrium moisture content, %; me is the specimen mass at moisture equilibrium, g; k is the reference mass: oven-dry mass for unmodified and pure-solvent groups, and the mass after conditioning at 25 ± 2 °C and 65 ± 5% RH (identical to m0) for modified groups, g. All *EMC* comparisons between groups were made after identical conditioning at 25 ± 2 °C and 65 ± 5% RH.

To evaluate the effect of modification on dimensional stability after moisture absorption, specimen dimensions before and after moisture absorption were measured with a vernier caliper. Fixed measuring points were marked on each specimen surface, and radial, tangential, and thickness dimensions were measured before impregnation and after moisture equilibrium, respectively, with a precision of 0.01 mm. Three replicate specimens were prepared for each group, and the results are reported as the arithmetic mean. The dimensional change rate in each direction

was calculated using Equation (4):

$$D = \frac{L_e - L_0}{L_0} \times 100\% \quad (4)$$

where D is the dimensional change rate in the corresponding direction, %; L_e is the dimension after moisture equilibrium in the corresponding direction, mm; L_0 is the initial dimension measured after stabilization at 25 ± 2 °C and 65 ± 5% RH but before impregnation in the corresponding direction, mm.

Dynamic moisture-absorption tests were conducted to characterize the moisture-absorption kinetics of modified wood and to clarify its absorption rate and capacity under high humidity. At a constant temperature of 25 ± 2 °C, specimens in the initial stable state were transferred to a preset environment of 80% RH. Specimen mass was measured at predefined intervals until moisture equilibrium was reached, with a weighing precision of 0.01 g. Three replicate specimens were used for each group. Cumulative moisture absorption per unit area was calculated using Equation (5):

$$M_t = \frac{m_t - m_s}{A} \quad (5)$$

where M_t is the cumulative moisture absorption per unit area at time t in g/m^2; m_t is the specimen mass at time t in g; m_s is the initial stable mass of the specimen in g; A is the total surface area of the specimen in m^2.

Humidity buffering performance was evaluated in 5 L airtight glass containers to simulate the microenvironment of a sealed display cabinet, at a constant temperature of 25 ± 0.5 °C. Optimally modified and untreated poplar specimens (50 mm radial × 50 mm tangential × 10 mm longitudinal) were prepared with three replicates per group. All specimens were preconditioned at 25 ± 2 °C and 65 ± 5% RH for 48 h to constant mass. The initial high humidity inside the container was generated by placing a saturated KCl solution (≈ 82% RH) prior to sealing. Once the specimen was introduced, the container was sealed immediately. The internal relative humidity was recorded at 10 min intervals for 24 h using a temperature–humidity data logger. An empty container served as the blank control. The peak humidity, 24 h equilibrium humidity, stabilisation time, and moisture buffering value (MBV) per unit mass were calculated to assess the microclimate regulation performance.

Humidity buffering performance and mass retention after cyclic aging. After the 60-day (30-cycle) wet–dry aging test, the optimally modified specimens were reconditioned at 25 ± 2 °C and 65 ± 5% RH for 48 h to constant mass, and their dry weight was recorded to calculate the post-cycling WPG. The humidity buffering test was then repeated following the same procedure as the pre-cycling evaluation. The MBV, peak humidity, 24 h equilibrium humidity, and stabilisation time after cycling were determined and compared with the pre-cycling values to quantify the

retention of humidity buffering performance.

This test was conducted on specimens prepared with the optimal impregnation process to assess long-term color stability under cyclic humidity conditions, simulating the service environments of museum display cabinets and relic storage rooms. All tests were performed at 25 ± 2 °C. Each wet-dry cycle lasted 48 h, consisting of 24 h moisture adsorption at 80% RH followed by 24 h desorption at 40% RH. Thirty complete cycles were performed over 60 days, and the total color difference ΔE^*_{ab} under 80% RH was measured after every two cycles, namely every 4 days. Before each measurement, specimens were conditioned at 25 ± 2 °C and 65 ± 5% RH for 24 h to ensure a uniform testing baseline. The color measurement precision was 0.01.

To measure the effects of wood substrate, additive dosage, and impregnation process on humidity-responsive color behavior, a colorimeter measured L^*, a^*, and b^* color-space parameters. The initial color value measured at 25 ± 2 °C and 65 ± 5% RH was used as the reference. Surface color was tested after the specimens reached moisture equilibrium, and the total color difference ΔE^*_{ab} was calculated according to CIE standards. The basic color features of the three wood substrates were compared in the preliminary test, and additive content and process parameters were analyzed in the single-factor and orthogonal experiments. Five evenly distributed points were selected on each specimen. Three replicate specimens were used for each group, and the results are given as the arithmetic mean.

Scanning electron microscopy was used to compare microstructural differences among the wood substrates and to analyze the loading state of functional components under the best modification process. In the preliminary experiment, cross-sectional morphologies of Chinese fir, paulownia, and poplar were observed to compare pore structure, fiber arrangement, and cell-wall characteristics, providing a microscale basis for substrate screening. In the orthogonal experiment, only specimens prepared with the best process were tested, and component attachment and pore filling were compared with the untreated substrate. After gold sputtering, specimens were observed in high-vacuum mode at an accelerating voltage of 5-10 kV. Typical morphologies were recorded at magnifications of 100×, 600×, and 2000×.

Fourier transform infrared spectroscopy was used to analyze changes in functional groups in wood under the best modification process, verify loading of the functional components, and explain the modification mechanism. Only the optimally modified specimens and the matching untreated substrates were tested as solid specimens by the attenuated total reflection method, with a wavenumber range of 4000-400 cm^{-1}, a resolution of 4 cm^{-1}, and 32 accumulated scans. Background correction was applied before measurement. Functional-group changes were analyzed by comparing changes in the positions and intensities of characteristic absorption peaks.

Results

Preliminary Experiment Results

Figure 3 presents the impregnation rate and weight percent gain of the three wood substrates.

For all tested species, the impregnation rate decreased rapidly during the initial stage and then gradually leveled off. The sharpest decline occurred during 0-2 h; after 4 h, the internal pores were close to saturation, so the impregnation rate changed little. At 0.5 h, the impregnation rates of *Paulownia* spp., *Populus* spp., and Chinese fir were 15.80, 12.62, and 8.65 g/(m²·h), respectively. After 6 h, these values decreased to 4.26, 3.49, and 2.71 g/(m²·h), with final WPG values of 12.74%, 9.65%, and 6.81%, respectively. The overall impregnation capacity followed the order *Paulownia* spp. > *Populus* spp. > Chinese fir. The well-developed pore architecture of *Paulownia spp*. provided high adsorption and retention of the ethanol-deionized water mixed solvent, so it maintained the highest impregnation rate and WPG throughout the impregnation cycle. Chinese fir, in contrast, had compact tissue structures and narrow pore channels, which resisted solvent infiltration and led to relatively low impregnation rate and WPG. The permeability of *Populus* spp. was intermediate between these two species.

After surface liquid was removed and all specimens were kept at room temperature for 24 h until the solvent evaporated, the WPG values of the three substrates were determined. The WPG values of Chinese fir, *Populus* spp., and *Paulownia* spp. were -0.19%, -0.24%, and -0.25%, respectively, showing a small negative gain. This was attributed to mild leaching of intrinsic wood extractives by volatile ethanol and deionized water during impregnation, and confirmed that the base solvent alone did not leave stable retained material inside the wood tissue.

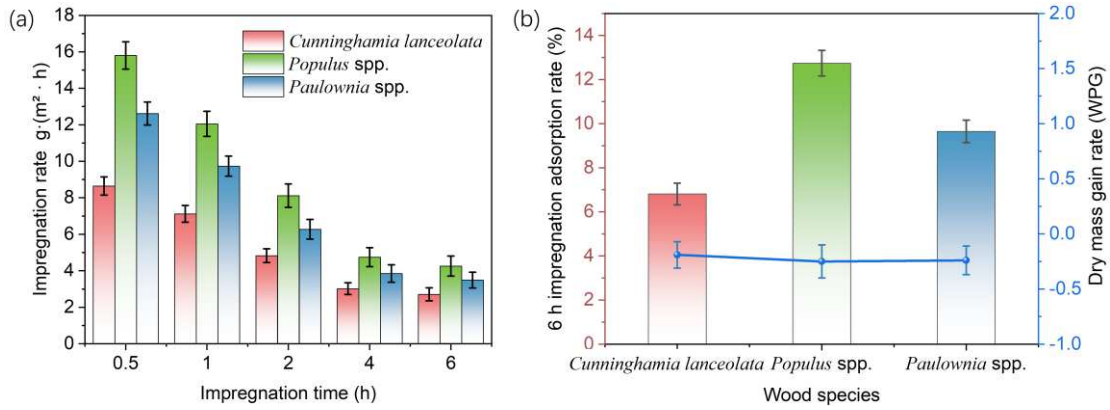


Fig. 3. Impregnation characteristics of three wood species at different impregnation durations. (a) Impregnation rate curves of *Cunninghamia lanceolata*, *Populus* spp. and *Paulownia* spp. within 0.5–6 h; (b) 6-hour impregnation rate and weight percent gain (WPG) of the three wood types (mean ± SD, $n = 3$).

Figure 4 shows the EMC and dimensional change of the three wood substrates after reaching moisture equilibrium at 80% RH. All specimens had the same dimensions of 50 mm (radial) × 50 mm (tangential) × 10 mm (longitudinal). The EMC values of Chinese fir, Populus spp., and Paulownia spp. were 8.09%, 10.41% ± 0.55%, and 12.58%, respectively, in the order *Paulownia* spp. > *Populus* spp. > Chinese fir. Moisture-induced swelling followed the inherent anisotropy of wood, and tangential change was greater than radial and longitudinal changes. The radial, tangential, and longitudinal dimensional change rates were 0.58%, 1.17%, and 0.08% for Chinese fir; 0.81%, 1.68% ± 0.15%, and 0.09% for *Populus* spp.; and 1.05%, 2.21%, and 0.12% for

Paulownia spp., respectively. These indicators showed the same ranking: *Paulownia* spp. > *Populus* spp. > Chinese fir.

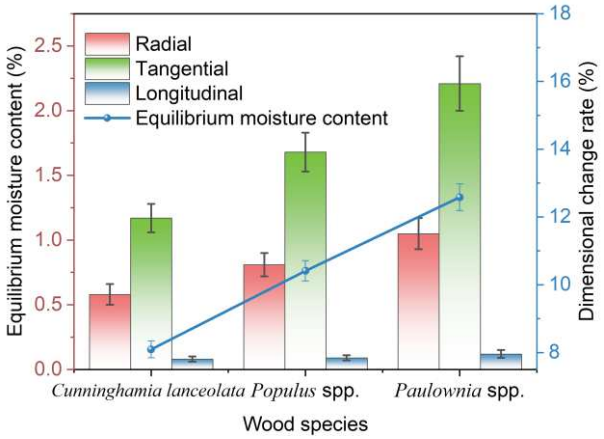


Fig. 4. Equilibrium moisture content (EMC) and radial, tangential and longitudinal dimensional change rates of *Cunninghamia lanceolata*, *Populus* spp. and *Paulownia* spp. (mean ± SD, n = 3).

Paulownia spp. had well-developed pore structures and abundant hydrophilic adsorption sites, which led to higher moisture absorption but also greater swelling. Chinese fir, by contrast, had compact fibrous bundles with strong cell-wall restraint, which limited moisture-induced swelling and gave excellent longitudinal dimensional stability.

The surface color parameters of Chinese fir, *Paulownia* spp., and *Populus* spp. after 6 h of impregnation in the ethanol-deionized water mixed solvent are shown in Table 7. During wetting, the L^* values of all three wood species decreased, which slightly darkened of the wood surface, while a^* and b^* changed little. After the specimens were kept at room temperature for 12 h to allow complete solvent evaporation, the color parameters almost returned to their initial values, and the total color difference ΔE^*_{ab} stayed below 0.22. This result shows that the pure solvent caused only reversible wetting-induced discoloration without permanent staining, and was chemically mild toward the wood surface.

Table 7 Changes in surface color parameters of three wood species before and after impregnation (mean ± SD, n = 3)

Wood species	Test state	L^*	a^*	b^*	ΔE^*_{ab}
Paulownia spp.	Initial	82.35 ± 0.42	0.82 ± 0.11	15.63 ± 0.24	0
	Impregnated	79.87 ± 0.45	0.95 ± 0.12	16.82 ± 0.26	2.15 ± 0.18
	12 h standing	82.18 ± 0.43	0.80 ± 0.11	15.59 ± 0.23	0.21 ± 0.05
Populus spp.	Initial	78.64 ± 0.39	2.17 ± 0.13	18.45 ± 0.27	0
	Impregnated	76.02 ± 0.41	2.31 ± 0.14	19.74 ± 0.29	2.38 ± 0.19
	12 h standing	78.52 ± 0.38	2.15 ± 0.13	18.40 ± 0.26	0.17 ± 0.06
Chinese fir	Initial	73.21 ± 0.37	5.89 ± 0.16	21.76 ± 0.31	0
	Impregnated	71.03 ± 0.39	6.02 ± 0.17	22.85 ± 0.33	2.07 ± 0.17
	12 h standing	73.06 ± 0.36	5.84 ± 0.15	21.68 ± 0.30	0.20 ± 0.06

SEM observations were conducted on the three wood substrates before and after pure-solvent

impregnation to evaluate the microstructural changes induced by the solvent system. As shown in Fig. 5, untreated poplar (a) exhibited a regular, straight fiber arrangement with a relatively uniform pore size distribution; paulownia (c) displayed wide vessels and an abundant porous network characteristic of broad-leaved species; and Chinese fir (e) presented the dense, elongated tracheid arrangement typical of softwoods, with a compact tissue structure.

After impregnation with the ethanol–deionized water mixed solvent, the fibrous skeleton and cell walls of all three species remained intact, as observed in poplar (b), paulownia (d), and Chinese fir (f), without visible cracking, fiber rupture, or structural collapse. This confirms that the low-temperature mixed-solvent system is chemically mild and does not compromise the wood matrix. Concurrently, the solvent treatment effectively removed the minor wood debris and dissolved the natural extractives originally attached to the inner pore walls, leaving cleaner and more open cell lumens.

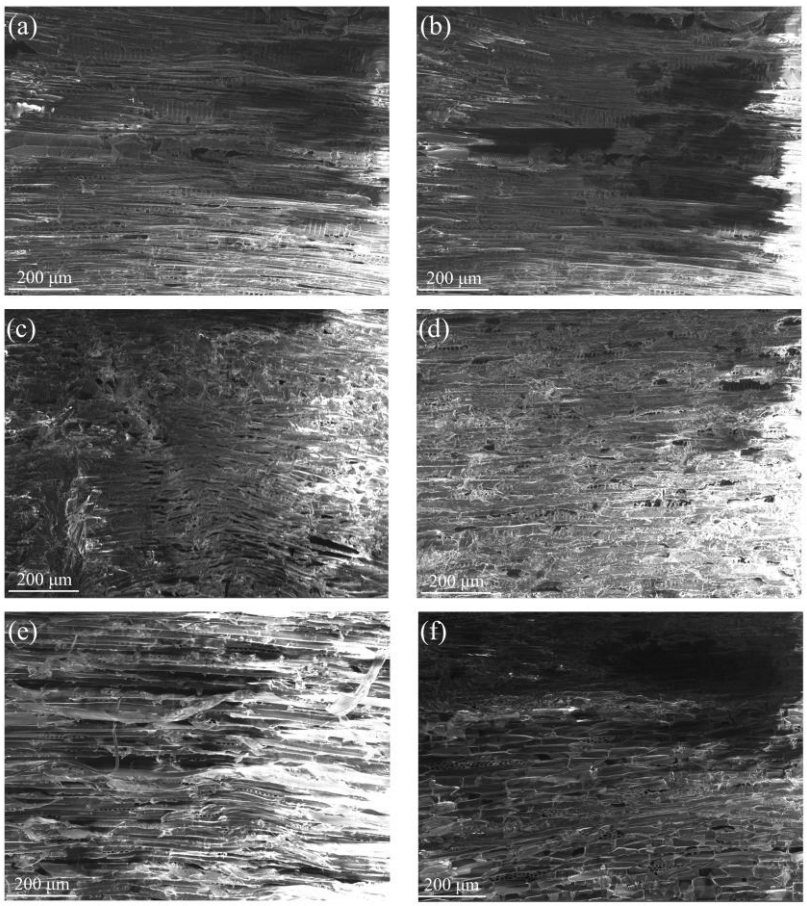


Fig. 5. SEM micrographs of three wood substrates before and after pure-solvent impregnation (500× magnification). (a) Untreated *Populus* spp.; (b) Solvent-impregnated *Populus* spp.; (c) Untreated *Paulownia* spp.; (d) Solvent-impregnated *Paulownia* spp.; (e) Untreated *C. lanceolata*; (f) Solvent-impregnated *C. lanceolata*.

Based on the preliminary indices, including impregnation rate, WPG, EMC, dimensional stability, and surface color difference, clear differences were observed among the three species

because of their inherent micropore structures. *Paulownia* spp. showed well-developed pores and therefore high solvent penetration and moisture-absorption capacity, but also greater swelling deformation. Chinese fir had compact tissue structures and excellent dimensional stability, but relatively low impregnation efficiency. By contrast, *Populus* spp. showed the most balanced overall performance, with uniform impregnation behavior and controllable swelling. In addition, only reversible color variation occurred after solvent impregnation, indicating stable surface appearance in poplar specimens. The wood pores were nearly saturated after 6 h of impregnation; therefore, this duration was used in the subsequent single-factor and orthogonal experiments. Considering the modification process, the requirement for humidity-responsive color indication, and the fact that poplar is a widely cultivated fast-growing timber in China, *Populus* spp. was selected as the substrate for all subsequent formal tests after comprehensive performance balancing [30].

Single-factor experimental results

To evaluate the influence of glycerol dosage on the overall performance of modified poplar wood, single-factor experiments were performed with the impregnation duration fixed at 6 h and the purple sweet potato anthocyanin content fixed at 0.5 wt%. The glycerol mass-fraction gradient was set at 20, 22, 24, 26, and 28 wt%. An untreated blank group, a pure-solvent control group, and a solvent-anthocyanin reference group were also established for comparison. The performance data obtained under different glycerol contents are shown in Fig. 6.

The weight percent gain (WPG) increased continuously with glycerol proportion, rising rapidly from 20 wt% to 24 wt% and then gradually slowing. The WPG of the pure-solvent group was -0.21 ± 0.27%, because the ethanol-deionized water mixed solvent slightly dissolved inherent water-soluble extractives and caused minor mass loss. The solvent-anthocyanin reference group showed a WPG of 0.42 ± 0.33%, because anthocyanins adsorbed onto the inner pore walls offset this mass loss and produced an overall positive gain. With 20 wt% glycerol, the WPG increased to 3.21 ± 0.54%, and the maximum value of 4.81 ± 0.80% was obtained at 28 wt% glycerol. As a nonvolatile component, glycerol can be retained in the wood tissue and increase specimen dry mass. However, excessive glycerol markedly increases the viscosity of the impregnation solution, impedes deep penetration of functional additives into the wood matrix, and slows further mass gain.

The EMC of the specimens increased steadily with glycerol dosage. The blank group had an EMC of 10.41 ± 0.55%, which increased to 12.81 ± 0.77% at 28 wt% glycerol. Dimensional change rates in all groups followed the typical anisotropic behavior of wood: tangential > radial > longitudinal. Dimensional deformation decreased slightly at 20-22 wt% glycerol and gradually increased when the glycerol mass fraction exceeded 22 wt%, whereas longitudinal dimensions remained stable. Glycerol partly filled wood pores and limited water ingress, thereby restraining swelling deformation. At high concentrations, however, its strong hygroscopicity increased overall

moisture absorption, and swelling became dominant. Specimens treated with 22 wt% glycerol had a tangential dimensional change rate of 1.59 ± 0.25%, 4.8% lower than that of blank specimens, indicating the best dimensional stability.

Using untreated poplar wood as the benchmark, the pure-solvent group showed a total color difference of only 0.78 ± 0.24, with no obvious visual difference, whereas the solvent-anthocyanin reference group showed a uniform pale tone with a ΔE^*_{ab} of 2.35 ± 0.35. The total color differences of the glycerol-gradient groups were 2.38 ± 0.31, 2.41 ± 0.30, 2.37 ± 0.32, 2.43 ± 0.33, and 2.39 ± 0.34 at 20, 22, 24, 26, and 28 wt%, respectively. Variation in glycerol content caused only minor fluctuations in L^*, a^*, and b^*, with total color difference remaining between 2.37 and 2.43. Because glycerol is colorless and transparent, it does not alter the inherent base color of wood or react with anthocyanins to produce color changes; therefore, its dosage has negligible influence on humidity-responsive color indication.

Comprehensive analysis showed that glycerol below 20 wt% resulted in insufficient loading of functional components and limited humidity-regulation performance, whereas glycerol above 28 wt% sharply increased solution viscosity and aggravated wood swelling deformation. By balancing moisture buffering capacity and dimensional stability, 22 wt% glycerol provided a favorable compromise, with good dimensional stabilization while maintaining adequate moisture-absorption capacity. This dosage was therefore selected as the central level for subsequent orthogonal experiments.

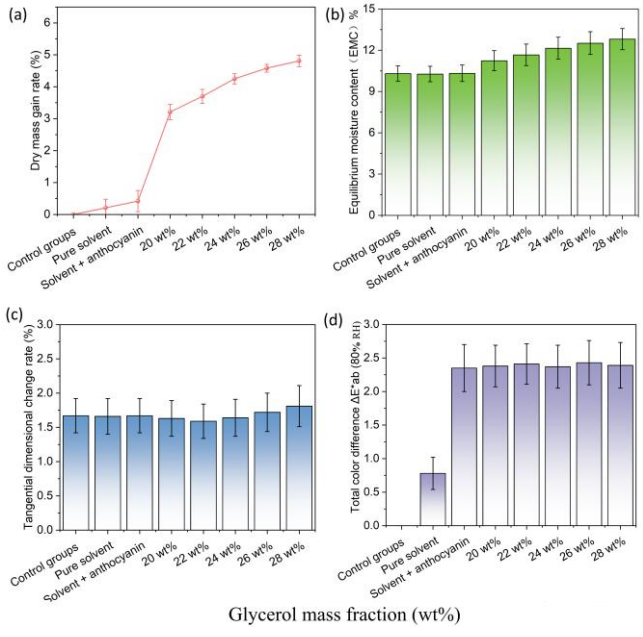


Fig. 6. Effects of glycerol mass fraction on mass gain, moisture absorption, dimensional stability and color performance of *Populus* spp. modified with anthocyanin. (**a**) Dry weight percent gain (WPG); (**b**) Equilibrium moisture content (EMC); (**c**) Tangential dimensional change rate; (**d**) Total color difference ΔE^*_{ab} under 80% relative humidity. (mean ± SD, n = 3).

To explore the effect of anthocyanin dosage on the multifunctional properties of modified

poplar wood, a fixed glycerol mass fraction of 22 wt% and an impregnation duration of 6 h were used. Anthocyanin concentration gradients of 0.2, 0.4, 0.6, 0.8, and 1.0 wt% were set, with an untreated blank group and a pure-glycerol modified reference group for comparison. The overall performance indices of modified poplar wood under different anthocyanin contents are presented in Figure 7.

Anthocyanin dosage had little effect on the WPG of the specimens. The WPG of the blank group was 0%. The pure-glycerol reference group exhibited a WPG of 3.70 ± 0.62%, which increased only slightly to 4.01 ± 0.79% when the anthocyanin dosage reached 1.0 wt%. Thus, glycerol dominated the overall loading of functional components, whereas changes in anthocyanin dosage did not clearly affect mass retention within the wood.

The EMC and dimensional stability of wood showed very small fluctuations with anthocyanin dosage. The EMC of the blank group was 10.41 ± 0.30%. The EMC of the pure glycerol group rose to 11.67 ± 0.75%, and EMC values of all groups concentrated between 11.66% and 11.72%, with no clear rising or falling trends relative to the pure glycerol reference group. Consistent with wood anisotropy, dimensional change rates followed the order tangential > radial > longitudinal. The tangential dimensional change rate of blank specimens was 1.68 ± 0.15%, while that of the pure glycerol group decreased to 1.59 ± 0.25%. Radial and tangential swelling fluctuations of all groups were less than 0.04%, and longitudinal dimensions remained nearly constant. As a small-molecule pigment, anthocyanin failed to alter glycerol's pore-filling effect, so the moisture uptake and swelling mechanism of wood remained unchanged.

For surface color and humidity-responsive performance, the initial color parameters measured at 25 °C and 65% RH were used as the benchmark. All specimens reached moisture equilibrium at 80% RH before color measurement. The pure-glycerol group showed a total color difference ΔE^*_{ab} of 0.81 ± 0.30, with almost no visual difference. ΔE^*_{ab} increased with anthocyanin mass fraction, from 1.47 ± 0.33 at 0.2 wt% to 2.87 ± 0.44 at the best dosage of 0.6 wt% and 4.15 ± 0.55 at 1.0 wt%. The surface color gradually deepened as pigment loading increased. Purple sweet potato anthocyanin is a pH-sensitive natural pigment. High humidity forms a thin liquid film on the wood surface and slightly changes the surface micro-pH, triggering reversible molecular structural transformation of anthocyanin and macroscopically darkening the wood color.

Although higher anthocyanin dosage produced a larger color-change amplitude, excessive pigment tended to accumulate along wood-grain depressions, reducing color uniformity among replicate specimens and increasing data dispersion. At low anthocyanin concentrations, the humidity response signal was too weak for identification inside sealed display cabinets; at excessively high dosages, the stronger initial background color could mask the dynamic color change induced by humidity. The 0.6 wt% anthocyanin group showed a moderate base tone and clear high-humidity color contrast, which was favorable for visual humidity identification, as shown in Fig. 8.

Comprehensive evaluation showed that anthocyanin dosages below 0.2 wt% failed to provide a sufficient color-rendering effect, whereas dosages above 1.0 wt% caused poor pigment dispersion and high data scatter. By balancing color sensitivity, surface uniformity, and humidity-recognition efficiency, 0.6 wt% was selected as the central level of anthocyanin, which matched well with the 22 wt% glycerol level for the following orthogonal optimization of the impregnation process.

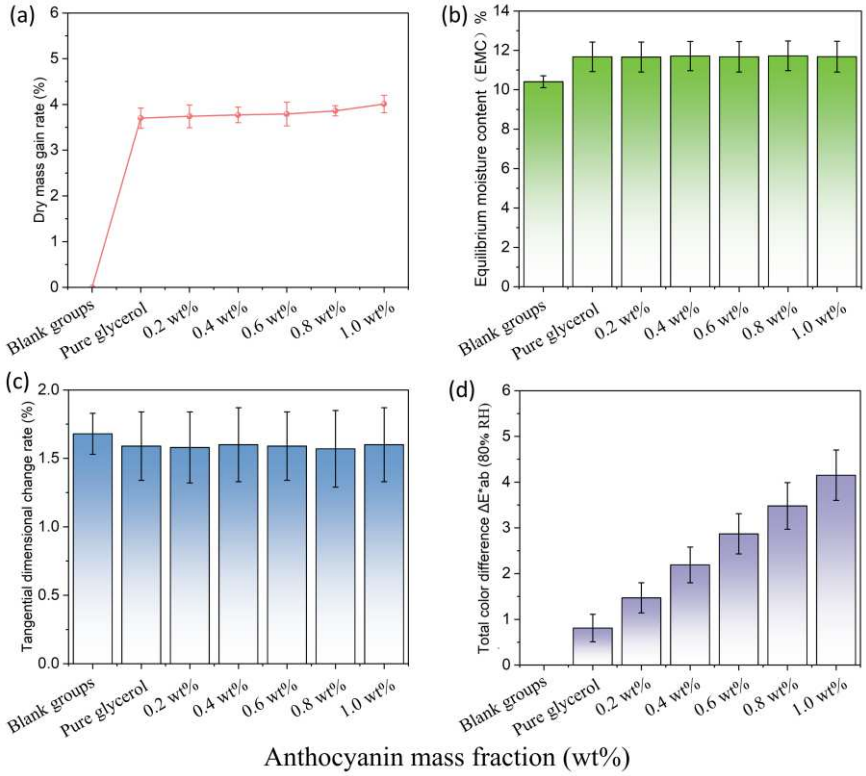


Fig. 7. Effects of purple sweet potato anthocyanin mass fraction on mass gain, moisture absorption, dimensional stability and color performance of glycerol-modified *Populus* spp. (a) Dry weight percent gain (WPG); (b) Equilibrium moisture content (EMC); (c) Tangential dimensional change rate; (d) Total color difference ΔE^*_{ab} under 80% relative humidity. (mean ± SD, n = 3).



Fig. 8. Macroscopic appearance of glycerol-modified *Populus* spp.

Orthogonal experimental results

On the basis of the above single-factor experimental findings, glycerol mass fraction (Factor

A), anthocyanin mass fraction (Factor B), and impregnation duration (Factor C) were selected as three influencing factors for the orthogonal test, with the total color difference at 80% RH set as the primary evaluation index and WPG and EMC taken as auxiliary indicators. Range analysis and one-way analysis of variance (ANOVA) were used to measure the effect magnitude of each factor and screen the best impregnation parameters, and the matching data are displayed in Tables 8 and 9.

Table 8. Orthogonal test results and range analysis (mean ± SD, n = 3)

No.	A (wt%)	B (wt%)	C (h)	WPG (%)	EMC (%)	Total ΔE^*_{ab}
1	21	0.5	3	3.42 ± 0.51	11.24 ± 0.61	2.51 ± 0.32
2	21	0.6	6	3.65 ± 0.54	11.47 ± 0.62	2.98 ± 0.41
3	21	0.7	9	3.76 ± 0.67	11.56 ± 0.75	3.49 ± 0.58
4	22	0.5	6	3.68 ± 0.55	11.62 ± 0.68	2.57 ± 0.35
5	22	0.6	9	3.89 ± 0.66	11.85 ± 0.72	3.04 ± 0.44
6	22	0.7	3	3.67 ± 0.63	11.68 ± 0.71	3.37 ± 0.53
7	23	0.5	9	3.92 ± 0.77	12.01 ± 0.78	2.63 ± 0.33
8	23	0.6	3	3.84 ± 0.64	11.91 ± 0.73	3.02 ± 0.44
9	23	0.7	6	4.08 ± 0.80	12.15 ± 0.82	3.52 ± 0.61
k_1	2.993	2.570	2.967			
k_2	2.993	3.013	3.023			
k_3	3.057	3.460	3.053			
R	0.064	0.890	0.086			

Note：k_1, k_2, k_3 are the mean values of ΔE^*_{ab} for each level; R denotes range.

Table 9. ANOVA of orthogonal test (mean ± SD, n = 3)

Factor	SS	DF	MS	F	Significance
A	0.031	2	0.016	0.07	Insignificant
B	3.429	2	1.715	7.89	Extremely significant
C	0.025	2	0.012	0.06	Insignificant
Error	3.932	18	0.218		
Total	7.417	26			

Note: Critical values $F_{0.05}(2,18)$ and $F_{0.01}(2,18)$ were adopted to judge significance. Effects with P<0.01 are extremely significant, while P>0.05 means no significant difference.

The range analysis showed that the influence of the three factors on total color difference followed the order B > C > A. The range value of Factor B (anthocyanin mass fraction) was substantially larger than those of Factor A (glycerol mass fraction) and Factor C (impregnation duration), indicating that anthocyanin mass fraction was the dominant factor governing the color-indicating performance of the modified wood. Glycerol mass fraction only slightly altered the surface micro-pH of the wood and thus exerted minor interference on color difference.

Extending the impregnation duration from 3 h to 9 h did not markedly increase anthocyanin loading and therefore produced no significant improvement in humidity-sensitive discoloration.

The ANOVA results in Table 9 were consistent with the range analysis. Only Factor B exhibited an extremely significant effect on total color difference, whereas Factor A and Factor C showed insignificant influences. The nearly equal k_1 and k_2 mean values of Factor A further verified that glycerol mass fraction barely affected the color-changing performance of specimens, consistent with the single-factor test results. Although preliminary experiments showed that wood pores could basically reach saturation after 6 h of impregnation, the glycerol–anthocyanin mixed impregnation solution has higher viscosity; extending the impregnation duration to 9 h facilitated deeper penetration of pigments and improved color uniformity; therefore, the 9 h group demonstrated better comprehensive performance.

Although range analysis of ΔE^*_{ab} indicated that Factor B was dominant, Factors A and C mainly governed WPG and EMC (Table 8). To balance color sensitivity, moisture buffering capacity, and dimensional stability, a multi-index weighted scoring method was employed: ΔE^*_{ab}, WPG, and EMC were normalized by the range method and assigned equal weights. Trial 5 ($A_2B_2C_3$: 22 wt% glycerol, 0.6 wt% anthocyanin, 9 h) achieved the highest composite score, combining satisfactory color response ($\Delta E^*_{ab} = 3.04$) with enhanced mass gain (WPG = 3.89%) and moisture uptake (EMC = 11.85%). This combination was therefore selected as the optimal process.

Performance of optimally modified specimens

Three groups of parallel specimens were prepared using the optimised impregnation parameters for verification tests. All specimens were first conditioned to moisture equilibrium at 25 ± 2 °C and 65% RH to obtain a uniform baseline. The measured WPG, EMC, and total colour difference at 80% RH were 3.82 ± 0.64%, 11.67 ± 0.72%, and 3.01 ± 0.41, respectively. All indicators deviated by less than 5% from the corresponding values of Group 5 in the orthogonal experiment, and the error ranges were consistent with the dispersion observed in previous tests, confirming the stability and repeatability of the impregnation process. Specimens prepared under this optimised condition were used for all subsequent characterisation, including dynamic moisture absorption, humidity buffering, cyclic aging, SEM, and FTIR analyses.

To characterize the moisture-absorption kinetics and humidity-responsive color behavior of modified wood at high humidity, all specimens were preconditioned to constant mass at 25 ± 2 °C and 65% RH to record the initial baseline color and mass. Simultaneous 24 h dynamic absorption and color-monitoring tests were then carried out on blank poplar specimens, pure-solvent controls, and optimally modified specimens at 25 ± 2 °C and 80% RH. Cumulative moisture uptake per unit area and total color difference ΔE^*_{ab} were recorded at regular intervals, and the matching results are presented in Figure 9.

All three groups showed the same moisture-absorption pattern: rapid adsorption at the early stage, followed by a gradual decrease in rate until equilibrium was reached. The absorption rate

peaked within 0-4 h, and the mass change of all specimens within 24 h was less than 0.2%, meeting the criterion for moisture equilibrium. Untreated poplar specimens and pure-solvent controls reached equilibrium at 12 h and 11 h, respectively, with 24 h unit-area moisture uptakes of 23.0 ± 1.9 g/m² and 22.1 ± 1.6 g/m². By contrast, the optimally modified specimens reached equilibrium after only 9 h, and their 24 h moisture uptake reached 35.0 ± 2.8 g/m², about 51% higher than that of blank poplar.

The color-response trend was consistent with moisture uptake, and color equilibrium occurred earlier than overall moisture saturation. The total color difference of the blank and pure-solvent groups remained below 0.8 throughout the test, arising only from small surface darkening caused by water wetting. For the modified specimens, ΔE^*_{ab} increased rapidly with moisture uptake and slowed after 8 h, finally stabilizing at 2.98 ± 0.42 at 24 h. These results demonstrate that the modified wood responds rapidly to elevated ambient humidity and can provide both passive humidity buffering and visual color indication. In Figure 10, the observed color darkening of the modified specimen under elevated humidity is consistent with the quantitative ΔE^*_{ab} value, confirming its feasibility as a passive visual humidity indicator.

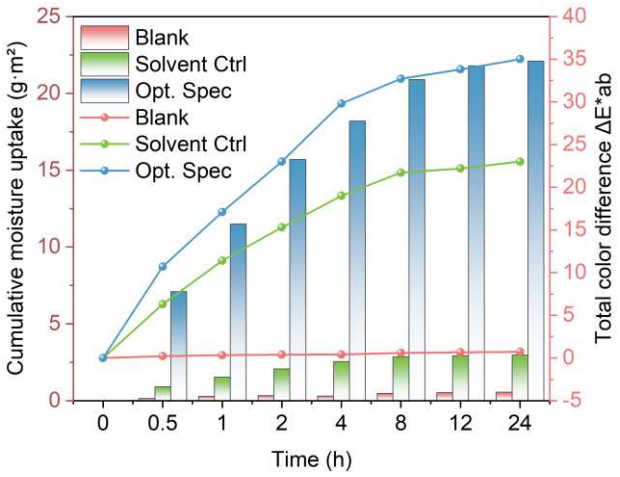


Fig. 9. Dynamic moisture absorption and color response curves of blank *Populus* spp., pure-solvent control and optimally modified specimens within 24 h under 80% relative humidity. (mean ± SD, n = 3).

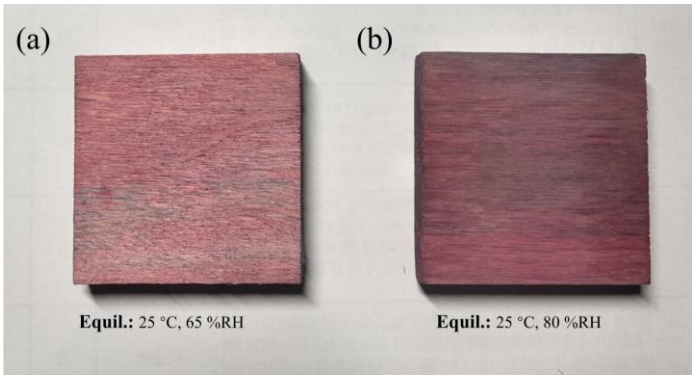


Fig. 10. Macroscopic color change of the optimally modified poplar specimen under different humidity equilibrium states. (a) Baseline state after equilibrium at 25 ± 2 °C, 65% RH; (b) High-humidity response state after equilibrium at 25 ± 2 °C, 80% RH.

549 The humidity buffering parameters of each group in the sealed containers are summarised in
550 Table 10. In the blank control, the internal humidity showed no significant attenuation and
551 remained at 81.2% RH after 24 h, indicating a negligible buffering effect. Untreated poplar
552 adsorbed a portion of the water vapour, with a peak humidity of 81.8% RH, a 24 h equilibrium
553 humidity of 72.5% RH, and a stabilisation time of approximately 14 h.

554 The optimally modified poplar exhibited significantly enhanced buffering performance: the
555 peak humidity decreased to 78.1% RH, the 24 h equilibrium humidity dropped to 67.3% RH, and
556 the stabilisation time was shortened to 9 h. The MBV per unit mass was approximately 49%
557 higher than that of untreated poplar. These results directly confirm that the modified wood can
558 effectively suppress abrupt humidity rises in enclosed spaces and deliver practical passive
559 microclimate regulation.

560 Table 10 Humidity buffering parameters of each group in sealed containers (mean ± SD, n = 3)

Group	Peak RH (%)	24 h equilibrium RH (%)	Stabilisation time (h)	24 h MBV (g/(kg·%RH))
Blank container	82.1 ± 0.3	81.2 ± 0.4	–	–
Untreated poplar	81.8 ± 0.5	72.5 ± 0.8	14.0 ± 0.9	0.72 ± 0.06
Optimally modified poplar	78.1 ± 0.6	67.3 ± 0.7	9.0 ± 0.6	1.07 ± 0.08

561 Note: MBV, moisture buffering value. "–" indicates that the parameter is not applicable.

562 The color durability of optimally modified specimens during 60-day wet-dry cyclic aging is
563 presented in Figure 11. All ΔE^*_{ab} values were measured under a uniform testing protocol:
564 specimens were conditioned at 25 ± 2 °C and 65 ± 5% RH for 24 h to restore the baseline state
565 after each cycle and were then re-equilibrated at 80% RH before color measurement, ensuring
566 consistent test conditions across all time points.

567 The uncycled optimally modified specimen was assigned a reference baseline of 0. During
568 the early aging stage from day 0 to day 20, ΔE^*_{ab} increased with the number of cycles, reaching
569 2.70 ± 0.37 on day 4 and peaking at 3.05 ± 0.58 on day 20. After day 20, the color responsiveness
570 gradually weakened under the combined effects of slow pigment leaching and oxidative
571 degradation, leading to a steady decline in total color difference, which decreased to 2.42 ± 0.46 at
572 the 60-day endpoint.

573 Throughout the 60-day cyclic aging process, the total color difference of all specimens
574 remained within a stable range of 2.42-3.05, without abrupt attenuation. This result shows that the
575 as-prepared modified wood has good medium- to long-term color-indicating durability and can
576 satisfy the service requirements of passive humidity indicators for enclosed cultural-heritage
577 exhibition spaces.

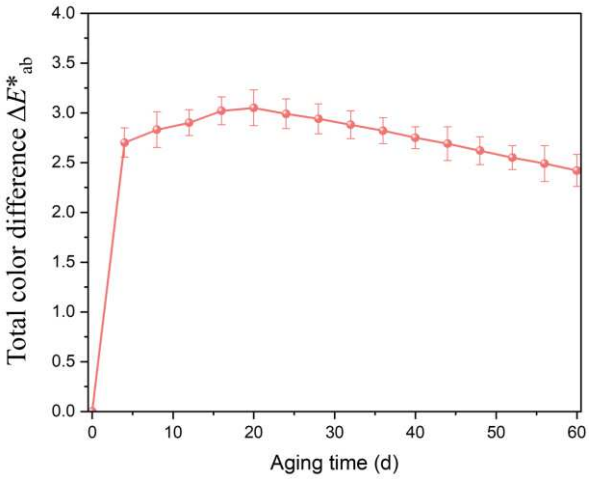


Fig. 11. Variation of total color difference ΔE^*_{ab} of optimally modified *Populus* spp. during 60-day dry-wet cyclic aging under 80% relative humidity.

The WPG and buffering performance of the optimally modified specimens were re-measured after the 60-day (30-cycle) wet–dry aging test and compared with the pre-cycling values (Table 11). The average WPG decreased from 3.82 ± 0.64% to 3.21 ± 0.58%, corresponding to a loss ratio of 16.0 ± 2.1%, indicating slow leaching of the impregnated components during the aging test.

The buffering performance attenuated in parallel: the MBV decreased from 1.07 ± 0.08 to 0.89 ± 0.07 g/(kg·%RH) (retention rate ≈ 83.2%), the 24 h equilibrium humidity rose from 67.3% to 69.5% RH, and the stabilisation time extended from 9.0 to 10.5 h. The close agreement between the WPG loss (16.0%) and the MBV decline confirms that glycerol leaching is the primary driver of the gradual reduction in humidity-buffering capacity. Overall, the material retained more than 80% of its buffering efficiency after 30 cycles, demonstrating stable medium- to long-term service capability.

Table 11 Changes in humidity buffering performance and mass of modified specimens before and after the 60-day (30-cycle) wet–dry aging test (mean ± SD, n = 3)

Index	Before cycling	After 30 cycles	Retention rate (%)
WPG (%)	3.82 ± 0.64	3.21 ± 0.58	84.0 ± 2.1
Peak RH (%)	78.1 ± 0.6	79.4 ± 0.7	–
24 h equilibrium RH (%)	67.3 ± 0.7	69.5 ± 0.8	–
Stabilisation time (h)	9.0 ± 0.6	10.5 ± 0.7	–
24 h MBV (g/(kg·%RH))	1.07 ± 0.08	0.89 ± 0.07	83.2 ± 2.4

Note: "–" indicates that retention rate is not applicable for this indicator. MBV, moisture buffering value.

SEM was used to examine the microstructure of untreated poplar, pure-solvent control, and optimally modified specimens at 500× and 1500× magnifications. The SEM images (Fig. 12) revealed that the fibrous skeletons and cell walls remained continuous and intact across all groups, with no signs of corrosion, fragmentation, or collapse, confirming that the low-temperature

ultrasonic impregnation caused no structural damage to the wood matrix.

Untreated poplar (Fig. 12a, 12b) exhibited open conducting tissues, smooth fiber walls, and hollow lumens, with only occasional natural dust particles. The control specimens (Fig. 12c, 12d) showed cleaner lumens due to extractive dissolution, but lacked nonvolatile components such as glycerol and anthocyanin, leaving no residue after solvent evaporation and pores predominantly hollow, largely indistinguishable from the untreated samples. In contrast, the optimally modified specimens (Fig. 12e, 12f) displayed distinct component deposition: gray-white aggregates within cell lumens at low magnification, and continuous films covering fiber walls and filling intercellular spaces at high magnification, with hollow areas markedly reduced. These morphological changes correlated well with the increases in WPG, EMC, and moisture absorption, confirming effective co-deposition of glycerol and anthocyanin within the wood pores. Pore densification and film coating provided additional water vapor adsorption sites and physically restrained cell-wall swelling, underpinning the enhanced moisture buffering and dimensional stability; meanwhile, the glycerol hydrogen-bonding network immobilises anthocyanin molecules within the wood matrix, mitigating pigment leaching and supporting durable colour response.

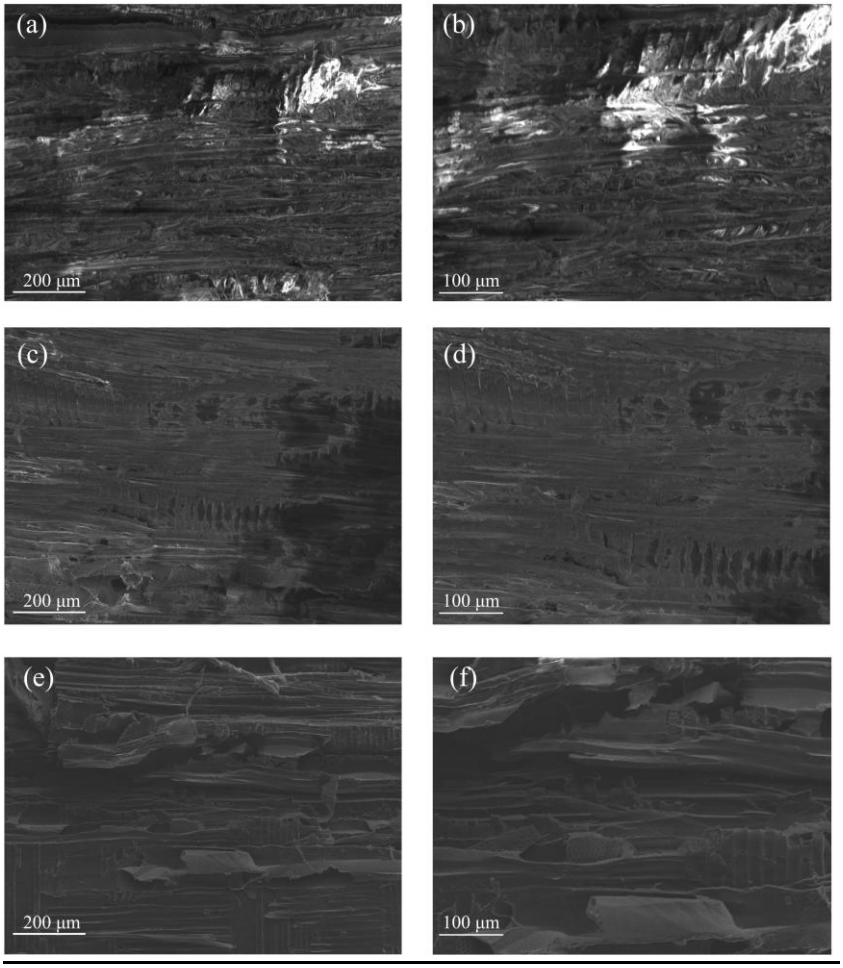


Fig. 12. SEM images of untreated poplar, pure-solvent control, and optimally modified specimens. (a)(b) Untreated Populus spp.; (c)(d) Pure-solvent control; (e)(f) Optimally modified specimens with glycerol and anthocyanin.

FTIR analysis was performed to characterize the chemical changes after modification. As shown in Fig. 13, the modified wood exhibited a significantly broader and deeper O-H absorption band at 3337 cm^{-1} compared to untreated poplar, indicating hydrogen bonding between the introduced hydroxyl groups (from glycerol and anthocyanin) and wood cell-wall polymers. The C-H stretching bands at 2919 and 2852 cm^{-1} showed a slight increase, consistent with the introduction of glycerol carbon skeletons. The band at 1736 cm^{-1}, assigned to the acetyl C=O stretching of hemicellulose, remained intact with no peak shift, confirming no degradation of the polysaccharide backbone. New or enhanced absorptions were observed at 1645 and 1591 cm^{-1}. The 1645 cm^{-1} band is attributed to the conjugated C=O stretching of the anthocyanin flavonoid nucleus (partially overlapped with the H-O-H bending of adsorbed water), while the 1591 cm^{-1} band is assigned to the aromatic C=C skeletal vibration of anthocyanin and syringyl units of lignin. The enhanced intensities at these bands confirmed the successful loading of anthocyanin with its chromophore preserved. Additional increases at 1238 and 1031 cm^{-1} further corroborated the incorporation of anthocyanin phenolic hydroxyls and glycerol polyhydroxy ethers. These spectral changes collectively confirm that glycerol and anthocyanin were co-loaded into poplar wood through pore filling and hydrogen-bonding interactions, without chemically altering the wood skeleton.

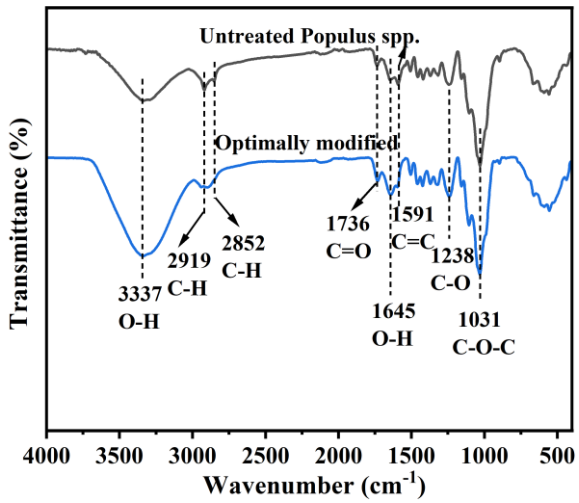


Fig. 13. FTIR spectra of untreated (gray) and optimally glycerol-anthocyanin modified (blue) poplar wood samples.

Discussion

This study addresses the limited availability of passive humidity-buffering materials that also provide visual humidity indication for enclosed museum exhibition spaces. To this end, poplar wood was modified through mild low-temperature ultrasonic co-impregnation with glycerol and anthocyanin. Under the optimised process (22 wt% glycerol, 0.6 wt% anthocyanin, 9 h impregnation), the modified wood exhibited a 51% higher 24 h moisture uptake than untreated poplar at 80% RH, while maintaining a reversible humidity-responsive colour change. The enclosed-chamber test (Table 10) further demonstrated that this enhanced moisture uptake

translates directly into microclimate regulation: the modified wood reduced the peak humidity by 4.0% RH and the 24 h equilibrium humidity by 5.2% RH relative to untreated wood, with an MBV approximately 49% higher. This confirms that the material can effectively suppress humidity surges in confined spaces, addressing the key practical requirement for passive humidity control in sealed display cabinets.

After 60 days of wet–dry cyclic aging, approximately 80% of the initial colour-indicating performance was retained. Post-cycling analysis (Table 11) revealed that the WPG decreased from 3.82% to 3.21% (loss ratio ≈ 16.0%) and the MBV declined from 1.07 to 0.89 g/(kg·%RH) (retention rate ≈ 83.2%). The close agreement between the WPG loss and the MBV attenuation confirms that the slow leaching of glycerol—the core hygroscopic component—is the primary driver of the gradual decline in both humidity-buffering capacity and colour response amplitude during the later stage of cycling. Importantly, the material retained more than 80% of its buffering efficiency after 30 cycles, demonstrating stable medium- to long-term service capability.

SEM observations demonstrated that the pores of the modified wood were effectively filled with glycerol–pigment complexes, and the intercellular spaces became narrower. These microstructural changes provided the physical basis for the enhanced moisture uptake and reduced dimensional deformation. FTIR results further confirmed the loading of functional components and their binding modes. The significant broadening of the O–H band at 3337 cm^{-1} verified the formation of extensive intermolecular hydrogen bonds between glycerol molecules and the hydroxyl groups of wood cellulose and hemicellulose. More importantly, the retention of the acetyl C=O band at 1736 cm^{-1} indicated no degradation of the polysaccharide backbone, consistent with the minimal-intervention principle for heritage conservation. This hydrogen-bonding network served two functions: it increased the number of water-vapour adsorption sites, thereby strengthening the humidity-buffering capacity, and it immobilises anthocyanin molecules within the wood matrix, reducing pigment leaching during wet–dry cycling and improving colour durability. The mildly acidic environment maintained by citric acid further stabilised the molecular structure of anthocyanins and retarded oxidative degradation. The weak acid may also have activated the surface hydroxyl groups of the wood, enhancing the binding strength between glycerol and the fibre matrix. Anthocyanin itself, as a small-molecule pigment, did not alter the pore structure of the wood and therefore had no significant effect on the humidity-buffering performance; its role was solely to realise the visual humidity response [32-35].

Compared with existing materials, which often provide either humidity regulation or colour indication alone, this system integrates both functions in a single wood-based substrate. The enclosed-chamber validation and post-cycling retention data further distinguish this work from studies that report only material-level moisture uptake without demonstrating practical microclimate regulation or component durability. The low-temperature ultrasonic process used here is mild and environmentally compatible, and it preserves the natural fibrous structure of wood, in line with the minimal-intervention principle of heritage conservation. Weak-acid pH

regulation and glycerol-matrix immobilisation further stabilise anthocyanin and support the dual functions of humidity buffering and colour indication, making the material more suitable for passive microclimate management in sealed display cabinets than conventional single-function materials [36].

Several limitations should also be noted. First, the optimized specimen produced a ΔE^*_{ab} of 3.01 ± 0.41 at 80% RH. According to the CIE-NBS criterion, this represents a perceptible color difference, but it is more suitable for close-range observation than for remote detection. This outcome reflects the relatively narrow humidity-response window of anthocyanin and the multi-index optimization strategy used here, which balanced dimensional stability, moisture buffering, and color sensitivity rather than maximizing color contrast alone. Second, although the enclosed-chamber test confirmed the material's ability to regulate ambient humidity under high-humidity conditions, complete adsorption–desorption cycling across a wider humidity range remains to be investigated. Third, the durability assessment was limited to wet–dry cycling at ambient temperature. Coupled aging factors such as light exposure, temperature variation, and long-term component leaching were not quantitatively evaluated.

Future work should focus on four aspects: (1) combining natural pigments to broaden the color-response range and improve the recognisability of humidity visualization; (2) completing bidirectional adsorption-desorption cycle tests to evaluate humidity buffering across the full humidity range; (3) improving component retention and aging resistance through wood pretreatment or fixation auxiliaries, followed by multi-factor aging tests; and (4) extending validation to additional wood substrates and refining the applicability evaluation system for different cultural relic conservation scenarios.

In summary, the modified wood developed in this study combines passive humidity buffering with reversible humidity-responsive colour indication through a green and mild preparation process. The enclosed-chamber test confirmed its practical microclimate regulation capability, and the post-cycling analysis demonstrated that over 80% of the buffering efficiency is retained after 30 wet–dry cycles. These results establish the material as a promising functional substrate for passive microclimate regulation in sealed museum display cabinets and historic buildings, with potential application in the preventive conservation of wooden cultural relics.

Data availability

All data generated or analyzed during this study are included in this article and its supplementary information files.

Acknowledgements

The authors thank Beijing Forestry University and the Palace Museum for providing experimental materials and samples, and appreciate the laboratory support from Northwestern Polytechnical University and Central South University of Forestry and Technology. No funding was received for this research.

References

1. Qu, X., et al. Timber species identification and selection principles of wooden components in the Sunjialou Cultural Relic Building, Nanyang City. *npj Heritage Science*, **14**, 1 (2026).
2. Zhang, L., Guo, Y. & Yang, C. Degradation and Protection of Wooden Cultural Relics: A Mini Review. *Coatings*, **15**, 12 (2025).
3. Pavlogeorgatos, G. Environmental parameters in museums. *Building and Environment*, **38**, 1457–1462 (2003).
4. Zhu, Y. The Phenomenon of Fragmentation of Architectural Heritage — On the Analysis of the Protection Form of Muta (Wooden Pagoda) Temple Relics Park. *Applied Mechanics and Materials*, **3309**, 584–586 (2014).
5. Yang, J. & Fu, M. Research on Non-Destructive Testing Technology in Conservation Repair Project of Ancestral Temple in Mukden Palace. ISPRS Annals of Photogrammetry, *Remote Sensing and Spatial Information Sciences*, **2**, 341–348 (2017).
6. Lappalainen, V., Sohlberg, E. & Pasanen, P. Simulation studies on the effect of microbial growth and moisture damaged materials on indoor air quality. *Building and Environment*, **301**, 114799 (2026).
7. Pagliaro, F., Bukowiecki, E., Gugliermetti, F., et al. The architecture of warehouses: A multidisciplinary study on thermal performances of Portus' roman store buildings. *Journal of Cultural Heritage*, **16**, 560–566 (2015).
8. Camuffo, D., Bertolin, C., Bonazzi, A., et al. Past, present and future effects of climate change on a wooden inlay bookcase cabinet: A new methodology inspired by the novel European Standard EN 15757:2010. *Journal of Cultural Heritage*, **15**, 26–35 (2014).
9. Paneru, D., Croyle, B., Wimmers, G., et al. Impact of climate change on hygrothermal durability of exterior, non-load-bearing mass timber wall. *Journal of Building Engineering*, **106**, 112558 (2025).
10. H., Y., S., W. K. & L., W. Performance analysis on thermal energy storage unit for an atmospheric water harvester in museum display case. *Journal of Energy Storage*, **52**, 137754 (2022).
11. Olek, W. & Bonarski, J. Texture changes in thermally modified wood. *Archives of Metallurgy and Materials*, **53**, 207–211 (2008).
12. Mourad, R., Rabah, D. & Dongxia, W. Experimental investigation of hygrothermal behavior of wooden-frame house under real climate conditions. *Energy and Built Environment*, **4**, 122–129 (2023).
13. Alessandra, U., Vincenzo, C., Francesco, N., et al. Moisture-Related Risks in Wood-Based Retrofit Solutions in a Mediterranean Climate: Design Recommendations. *Sustainability*, **14**, 111934 (2022).
14. Cho, M. H., Wi, S., Chang, J. S., et al. Hygrothermal properties analysis of cross-laminated timber wall with internal and external insulation systems. *Journal of Cleaner Production*, **231**, 1353–1363 (2019).
15. Alaa, A. & Ibrahim, M. Preventing mold growth and maintaining acceptable indoor air quality for educational buildings operating with high mechanical ventilation rates in hot and humid climates. Air Quality, *Atmosphere & Health*, **16**, 341–361 (2022).

16. Papandrea, F. S., Zumbo, A., Mammoliti, A., et al. Effects of steaming treatment on the technological properties of olive wood. *European Journal of Wood and Wood Products*, **84**, 66 (2026).
17. Shabir, S., Dutt, B., Kumar, R., et al. Enhanced strength and chemical stability of Salix tetrasperma wood through thermal modification. *Scientific Reports*, **15**, 43208 (2025).
18. Doczekalska, B., Wencek, S. A., Bujnowicz, K., et al. Enhancing Functional and Visual Properties of Paulownia Wood Through Thermal Modification in a Steam Atmosphere. *Polymers*, **17**, 2000 (2025).
19. Ligne, D. L., Fredriksson, M., Thygesen, G. L., et al. Influence of degradation products from thermal wood modification on wood-water interactions. *Journal of Materials Science*, **60**, 1–19 (2025).
20. Sosins, G., Grinins, J., Brazdausks, P., et al. Aspen Wood Characteristics Following Thermal Modification in Closed Process Under Pressure in Nitrogen. *Materials*, **17**, 5930 (2024).
21. Ran, Y., Li, J., Zhang, S., et al. Super-stable modified wood for enhanced autonomous indoor humidity regulation. *Chemical Engineering Journal*, **488**, 150814 (2024).
22. E., J., Ridwansyah & E., Y. Color stability of anthocyanin extract from wastewater of purple sweet potato starch processing. IOP Conference Series: *Earth and Environmental Science*, **94**, 1241 (2023).
23. Jieyu, Z., Yujie, Y. & Rongzhen, L. Sugar reduction process of purple sweet potato concentrated juice by microbial fermentation for improved performance of natural pigments. *Biochemical Engineering Journal*, **191**, 638–641 (2023).
24. Fang, J., Lai, Q., Zhang, H., et al. Influence of materials and surface parameters on the moisture buffering in office buildings: A sensitivity analysis of China. *Case Studies in Thermal Engineering*, **61**, 104964 (2024).
25. Valeria, C., Eric, C. H., Daniel, M., et al. Moisture Buffering in Surface Materials Due to Simultaneous Varying Relative Humidity and Temperatures: Experimental Validation of New Analytical Formulas. *Applied Sciences*, **10**, 7665 (2020).
26. GB/T 1927.4-2021, Test methods for physical and mechanical properties of small clear wood specimens — Part 4: Determination of moisture content, *Standardization Administration of China*, Beijing (2021).
27. EN 14734:2022, Durability of wood and wood-based products — Determination of treatability of timber species to be impregnated with wood preservatives — Laboratory method, *European Committee for Standardization*, Brussels (2022).
28. Castañeda-Ovando, A., Pacheco-Hernández, L. D. M., Páez-Hernández, E. M., et al. Chemical studies of anthocyanins: A review. *Food Chemistry*, **113**, 859–871 (2008).
29. Torskangerpoll, K. & Andersen, M. Ø. Colour stability of anthocyanins in aqueous solutions at various pH values. *Food Chemistry*, **89**, 427–440 (2004).
30. Yang, H., Yu, L. & Wang, L. Effect of moisture content on the ultrasonic acoustic properties of wood. *Journal of Forestry Research*, **26**, 753–757 (2015).
31. Wang, B., Feng, M. & Zhan, H. Improvement of wood properties by impregnation with TiO2 via ultrasonic-assisted sol–gel process. *RSC Advances*, **4**, 56355–56360 (2014).

32. Engelund, E. T. & Maria, F. Wood Modification as a Tool to Understand Moisture in Wood. *Forests*, **12**, 372 (2021).
33. Mantanis, I. G., Young, A. R. & Rowell, M. R. Swelling of Wood. Part II. Swelling in Organic Liquids. Holzforschung - International Journal of the Biology, Chemistry, *Physics and Technology of Wood*, **48**, 480–490 (2009).
34. Cortez, R., Luna-Vital, A. D., Margulis, D., et al. Natural Pigments: Stabilization Methods of Anthocyanins for Food Applications. *Comprehensive Reviews in Food Science and Food Safety*, **16**, 180–198 (2017).
35. Engelund, T. E., Thygesen, G. L., Svensson, S., et al. A critical discussion of the physics of wood–water interactions. *Wood Science and Technology*, **47**, 141–161 (2013).
36. D'Orazio, M. & Maracchini, G. An experimental investigation on the indoor hygrothermal environment of a reinforced-EPS based temporary housing solution. *Energy and Buildings*, **204**, 109500 (2019).

Author information

Central South University of Forestry and Technology, Changsha, 410004, China
Lin Shi, Ting He, Li Zeng
The Palace Museum, Beijing 100009, China
Guangyao Cui
Corresponding author, Li Zeng, E-mail: t19911929@csuft.edu.cn

Author contributions

Conceptualization, L.S.; methodology, T.H.; validation, G.Y.C.; investigation, L.Z.; Writing - Original Draft, L.S.; Writing - Review & Editing, T.H., G.Y.C.; Visualization, L.S. Correspondence to Li Zeng. All authors have read and agreed to the published version of the manuscript.

Competing interests

The authors declare no competing financial or non-financial interests.

Figure legend

Fig. 1. Flowchart illustrating the fabrication procedure of multifunctional modified wood. Porous wood substrates including Chinese fir, paulownia and poplar were used as raw materials.

Fig. 2. Macro surface morphology of three wood substrates. (**a**) *Paulownia* spp.; (**b**) *Populus* spp.; (**c**) *Cunninghamia lanceolata* (Chinese fir).

Fig. 3. Impregnation characteristics of three wood species at different impregnation durations. (a) Impregnation rate curves of *Cunninghamia lanceolata*, *Populus* spp. and *Paulownia* spp. within 0.5–6 h; (b) 6-hour impregnation rate and weight percent gain (WPG) of the three wood types (mean ± SD, $n = 3$).

Fig. 4. Equilibrium moisture content (EMC) and radial, tangential and longitudinal dimensional change rates of *Cunninghamia lanceolata*, *Populus* spp. and *Paulownia* spp. (mean ± SD, $n = 3$).

Fig. 5. SEM micrographs of three wood substrates before and after pure-solvent impregnation (500× magnification). (**a**) Untreated *Populus* spp.; (**b**) Solvent-impregnated *Populus* spp.; (**c**)

Untreated *Paulownia* spp.; (**d**) Solvent-impregnated *Paulownia* spp.; (**e**) Untreated *C. lanceolata*; (**f**) Solvent-impregnated *C. lanceolata*.

Fig. 6. Effects of glycerol mass fraction on mass gain, moisture absorption, dimensional stability and color performance of *Populus* spp. modified with anthocyanin. (**a**) Dry weight percent gain (WPG); (**b**) Equilibrium moisture content (EMC); (**c**) Tangential dimensional change rate; (**d**) Total color difference ΔE^*_{ab} under 80% relative humidity. This single-factor experiment set three glycerol-free control groups, namely untreated blank specimens, pure-solvent control group (prepared with base solvent only) and reference group (base solvent with fixed anthocyanin). Glycerol mass fractions ranged from 20 wt% to 28 wt%. The anthocyanin dosage and impregnation duration were kept consistent for all samples (mean ± SD, n = 3).

Fig. 7. Effects of purple sweet potato anthocyanin mass fraction on mass gain, moisture absorption, dimensional stability and color performance of glycerol-modified *Populus* spp. (**a**) Dry weight percent gain (WPG); (**b**) Equilibrium moisture content (EMC); (**c**) Tangential dimensional change rate; (**d**) Total color difference ΔE^*_{ab} under 80% relative humidity. In this single-factor test, glycerol mass fraction was fixed at 22 wt%. Test groups included untreated blank group, pure glycerol control group (prepared with base solvent and glycerol without anthocyanin) and anthocyanin gradient groups ranging from 0.2 wt% to 1.0 wt% (mean ± SD, n = 3).

Fig. 8. Macroscopic appearance of glycerol-modified *Populus* spp. with different mass fractions of purple sweet potato anthocyanins. From left to right and top to bottom: blank group, pure glycerol group, 0.2 wt%, 0.4 wt%, 0.6 wt%, 0.8 wt%, 1.0 wt% anthocyanins. All specimens reached moisture equilibrium at 25 °C, 65% RH prior to photography.

Fig. 9. Dynamic moisture absorption and color response curves of blank *Populus* spp., pure-solvent control and optimally modified specimens within 24 h under 80% relative humidity. The bar graph stands for cumulative unit-area moisture absorption, and the line graph reflects time-varying total color difference ΔE^*_{ab}. The blank group is untreated poplar wood; the pure-solvent control (Solvent Ctrl) was only impregnated with base solvent without glycerol and anthocyanins; Opt. Spec refers to specimens prepared by the optimal impregnation formula of 22 wt% glycerol + 0.6 wt% anthocyanin. After 24 h of moisture adsorption, the moisture uptake of optimally modified samples was about 51% higher than that of blank wood (mean ± SD, n = 3).

Fig. 10. Macroscopic color change of the optimally modified poplar specimen under different humidity equilibrium states. (**a**) Baseline state after equilibrium at 25 ± 2 °C, 65% RH; (**b**) High-humidity response state after equilibrium at 25 ± 2 °C, 80% RH. The same specimen was photographed under identical lighting and background conditions to ensure comparability.

Fig. 11. Variation of total color difference ΔE^*_{ab} of optimally modified *Populus* spp. during 60-day dry-wet cyclic aging under 80% relative humidity. Each complete cycle includes 24 h moisture adsorption at 80% RH and 24 h desorption at 40% RH, and a total of 30 cycles were carried out. The total color difference was measured every two cycles (mean ± SD, n = 3).

Fig. 12. SEM images of untreated poplar, pure-solvent control, and optimally modified specimens. (**a**)(**b**) Untreated *Populus* spp.; (**c**)(**d**) Pure-solvent control; (**e**)(**f**) Optimally modified specimens with glycerol and anthocyanin. Left column (**a**, **c**, **e**): 500× (scale bar = 200 μm); right column (**b**,

876 **d**, **f**): 1500× (scale bar = 100 μm).

877 **Fig. 13.** FTIR spectra of untreated (gray) and optimally glycerol-anthocyanin modified (blue)
878 poplar wood samples. The modified wood exhibits a broader O–H band (3337 cm^{-1}) and enhanced
879 aromatic C=C/C=O absorptions (1591/1645 cm^{-1}), confirming the successful co-loading and
880 hydrogen-bonding immobilisation of anthocyanin and glycerol within the wood structure, without
881 chemically altering the main wood skeleton (1736 cm^{-1}).

Supplementary Files

This is a list of supplementary files associated with this preprint. Click to download.

- Table1.docx
- Table2.docx
- Table3.docx
- Table4.docx
- Table5.docx
- Table6.docx
- Table7.docx
- Table8.docx
- Table9.docx
- Table10.docx
- Table11.docx